Characterization of Physicochemical and Thermal Properties of Chitosan And Sodium Alginate after Biofield Treatment

Snehasis Jana, Mahendra Kumar Trivedi, Rama Mohan Tallapragada, Alice Branton, Dahryn Trivedi, Gopal Nayak, Rakesh Mishra

Pharmaceutica Analytica Acta

Trivedi et al., Pharm Anal Acta 2015, 6:10
http://dx.doi.org/10.4172/2153-2435.1000430

Research Article Open Access

Characterization of Physicochemical and Thermal Properties of Chitosan and Sodium Alginate after Biofield Treatment

Snehasis Jana[1*], Mahendra Kumar Trivedi[1], Rama Mohan Tallapragada[1], Alice Branton[1], Dahryn Trivedi[1], Gopal Nayak[1] and Rakesh Kumar Mishra[2]

[1]*Trivedi Global Inc., 10624 S Eastern Avenue Suite A-969, Henderson, NV 89052, USA*
[2]*Trivedi Science Research Laboratory Pvt. Ltd., Hall-A, Chinar Mega Mall, Chinar Fortune City, Hoshangabad Rd., Bhopal- 462026, Madhya Pradesh, India*

Abstract

Chitosan (CS) and sodium alginate (SA) are two widely popular biopolymers which are used for biomedical and pharmaceutical applications from many years. The objective of present study was to study the effect of biofield treatment on physical, chemical and thermal properties of CS and SA. The study was performed in two groups (control and treated). The control group remained as untreated, and biofield treatment was given to treated group. The control and treated polymers were characterized by Fourier transform infrared (FT-IR) spectroscopy, CHNSO analysis, X-ray diffraction (XRD), particle size analysis, differential scanning calorimetry (DSC) and thermogravimetric analysis (TGA). FT-IR of treated chitosan showed increase in frequency of –CH stretching (2925→2979 cm^{-1}) vibrations with respect to control. However, the treated SA showed increase in frequency of –OH stretching (3182→3284 cm^{-1}) which may be correlated to increase in force constant or bond strength with respect to control. CHNSO results showed significant increase in percentage of oxygen and hydrogen of treated polymers (CS and SA) with respect to control. XRD studies revealed that crystallinity was improved in treated CS as compared to control. The percentage crystallite size was increased significantly by 69.59% in treated CS with respect to control. However, treated SA showed decrease in crystallite size by 41.04% as compared to control sample. The treated SA showed significant reduction in particle size (d_{50} and d_{99}) with respect to control SA. DSC study showed changes in decomposition temperature in treated CS with respect to control. A significant change in enthalpy was observed in treated polymers (CS and CA) with respect to control. TGA results of treated CS showed decrease in T_{max} with respect to control. Likewise, the treated SA also showed decrease in T_{max} which could be correlated to reduction in thermal stability after biofield treatment. Overall, the results showed that biofield treatment has significantly changed the physical, chemical and thermal properties of CS and SA.

Keywords: Biofield treatment; Chitosan; Sodium alginate; Fourier transform infrared spectroscopy; X-ray diffraction; Particle size analysis; Thermal analysis

Abbreviations: CS: Chitosan; SA: Sodium alginate; XRD: X-Ray Diffraction; DSC: Differential Scanning Calorimetry; TGA: Thermogravimetric Analysis: TGA; FT-IR: Fourier Transform Infrared

Introduction

Pharmaceutical scientists have used polymers in every aspect of their work; for example polystyrene vials, rubber closures, plastic tubing for injection sets, and polyvinylchloride flexible bags to hold blood and intravenous solutions. The conventional use of polymers is often limited to packaging rather than drug delivery. Subsequently, the union of polymer and pharmaceutical sciences led to the introduction of polymer in the design and development of drug delivery systems [1]. Especially, targeted drug delivery is more promising approach where the drug can be transported more effectively from a dosage form to targeted organ in required concentration thereby minimizing the drug induced toxicity. As the oral route is most popular route of administration, a large emphasis has been devoted to the development of controlled oral drug delivery systems. However, the highly hydrophilic nature and short half-life (elimination half-life 2-3 hour) of drugs causes them to readily absorbed and eliminated [2]. This requires frequent dosing that lead to a decrease in patient compliance and further increase chances of severe side effects due to dose dumping [3]. This warrants extensive research to alleviate these drug side effects by fabricating novel polymer-based drug delivery devices.

In general, polymers are classified in several ways; but according to the simplest classification used for pharmaceutical purposes they are divided into natural and synthetic polymers. Polysaccharides as natural polymers have been commonly used for the development of controlled release dosage forms and sustained release formulations [4-6].

Chitosan (CS) is an excellent cationic biopolymer which can interact effectively with negatively charged polymers, macromolecules, and poly ions. CS based matrices are extensively investigated for oral, transdermal, rectal, and ocular drug delivery systems [7]. CS can be used as an effective targeted delivery to the upper part of gastro intestinal tract and stomach to improve bioavailability. Recently CS and SA based matrix tablets were formulated for controlled delivery of trimetazidine hydrochloride [8].

Sodium alginate (SA) is a well-known natural polymer of plant origin; it is mainly composed of (1-4) linked β-D-manuronic acid and α-L-guluronic acid units [9,10]. It has outstanding gel forming ability, biocompatibility and biodegradability which makes it a suitable candidate for biomedical, controlled release applications and matrices

***Corresponding author:** Snehasis Jana, Trivedi Global Inc., 10624 S Eastern Avenue Suite A-969, Henderson, NV 89052, USA, Tel: +91-755-6660006; E-mail: publication@trivedisrl.com

Received August 06, 2015; **Accepted** October 06, 2015; **Published** October 09, 2015

Citation: Jana S, Trivedi MK, Tallapragada RM, Branton A, Trivedi D, Nayak G, et al. (2015) Characterization of Physicochemical and Thermal Properties of Chitosan and Sodium Alginate after Biofield Treatment. Pharm Anal Acta 6: 430. doi:10.4172/21532435.1000430

for enzyme immobilization, etc. [11,12]. Moreover, SA can be cross linked with multivalent cations such as calcium ions which can lead to the formation of insoluble calcium alginate [13,14]. Due to this unique crosslinking nature SA shows reduced swelling in different solvents, resulting in minimized permeation of different solutes. This allows drug embedded alginate matrices to be used as sustained release formulations for controlled drug delivery applications [15-18].

Nevertheless, more hydrophilic nature of these polymers, sometime leads to premature release of the drugs leading to reduced bioavailability and efficacy. Therefore CS and SA polymer need to be properly modified in order to tailor its stability which can improve bioavailability of encapsulated drugs. Hence, in current research work an attempt was made to modify physicochemical properties of CS and SA through biofield treatment.

Biofield is a cumulative effect of electric and magnetic field induced by a human body on external surroundings. Thus, human beings have the ability to harness the energy from environment/Universe and can transmit into any object (living or non-living) around the Globe. The object(s) always receive the energy and respond into a useful manner that is called biofield energy. This whole process is known as biofield treatment. Recently, it was reported that a robotic quad copter can be controlled through the power of thoughts [19]. Mr. Trivedi is known to transform the physical and structural properties at the atomic level of various living and non-living things through his biofield treatment (The Trivedi Effect®). The said treatment has substantially changed the atomic and thermal properties of metals [20-23]. The biofield treatment has significantly changed the energy in the crystal as well as crystallite size and distance between the atoms in a unit cell. Furthermore, when biofield was exposed to diamond, graphite and activated charcoal, the treatment has caused substantial elongation and fracture to smaller particles, which confirmed that the biofield energy has acted at the polycrystalline level causing deformation of metal particles [22].

It has been recently published that the effect of Mr Trivedi's biofield treatment resulted in significant improvement of the yield and quality of various agriculture products [24-27]. It causes an increase in growth and anatomical characteristics of a herb *Pogostemon cablin* that is commonly used in perfumes, in incense/insect repellents, and alternative medicine [28]. Moreover, in microbiology, biofield treatment has also caused changes in the antibiotic susceptibility patterns and biochemical reactions that further induced changes in the characteristics of pathogenic microbes [29-31].

By considering above mentioned excellent outcomes from biofield treatment and properties of CS and SA, this work was undertaken to investigate the impact of biofield treatment on physical, chemical and thermal properties of CS and SA.

Materials and Method

Chitosan (CS) and sodium alginate (SA) has been procured from Sigma Aldrich, USA. The samples were divided into two parts; one was kept as control sample, while the other was subjected to Mr. Trivedi's biofield treatment and coded as treated sample. The treatment group was in sealed pack and handed over to Mr. Trivedi for biofield treatment under laboratory condition. Mr. Trivedi provided the treatment through his energy transmission process to the treated group without touching the sample. The control and treated samples were characterized by FT-IR, CHNSO, XRD, particle size, DSC, and TGA.

Characterization

Fourier transform infrared (FT-IR) spectroscopy: The infrared spectra of polymers (CS and SA) were recorded in the range of 500-4000 cm^{-1} with Perkin Elmer, Fourier Transform Infrared (FT-IR) Spectrometer, USA.

CHNSO analysis: The control and treated samples of CS and SA were analysed using CHNSO Analyser (Model Flash EA 1112 series), Thermo Finnigan Italy.

X-ray diffraction (XRD) study: XRD of control and treated polymer samples (CS and SA) were analysed by using Phillips Holland PW 1710 X-ray diffractometer system. The wavelength of the radiation was 1.54056 Å. The data was obtained in the form of 2θ versus intensity (a.u) chart. The obtained data was used for calculation of crystallite size using the following formula.

Crystallite size = $k\lambda/b \cos \theta$

Where λ is the wavelength and k is the equipment constant with a value of 0.94. Percentage change in crystallite size was calculated using following formula:

Percentage change in crystallite size = $[(G_t-G_c)/G_c] \times 100$

Where, G_c and G_t are crystallite size of control and treated powder samples respectively.

Particle size analysis

The average particle size and particle size distribution were analysed by using Sympetac Helos-BF Laser Particle Size Analyser with a detection range of 0.1 µm to 875 µm. Average particle size (d_{50}) and d_{99} size exhibited by 99% of powder particles were computed from laser diffraction data table. The percent change in d_{50} and d_{99} values were calculated by following formula.

Percentage change in d_{50} size = 100 x (d_{50} treated- d_{50} control)/d_{50} control

Percentage Change in d_{99} size = 100 x (d_{99} treated- d_{99} control)/d_{99} control

Differential scanning calorimetry (DSC): DSC of the polymer samples (CS and SA) were analysed by using Pyris-6 Perkin Elmer Differential Scanning Calorimeter (DSC) at a heating rate of 10°C / min under air atmosphere and air was flushed at a flow rate of 5 mL/ min. The treated sample was divided in two parts T1 and T2 for DSC analysis.

Thermogravimetric/ derivative thermogravimetry (TGA/DTG) analysis: The thermal stability of the polymer all samples were analysed by using Mettler Toledo simultaneous thermogravimetric/derivative thermogravimetry analyser (TGA/DTG). The samples were heated from room temperature to 400°C with a heating rate of 5°C /min under air atmosphere. The treated sample was divided in two parts T1 and T2 for TGA analysis.

Results and Discussion

FT-IR spectroscopy

FT-IR spectra of control and treated polymer samples of CS and SA are illustrated in Fig 1 and 2, respectively. FT-IR spectrum of control CS showed (Figure 1) presence of intense peaks at 1652 cm^{-1} which was due to amide-I stretching vibration in the sample. FT-IR spectrum of CS showed stretching peak at 3434 and 2925 cm^{-1} for –OH and –

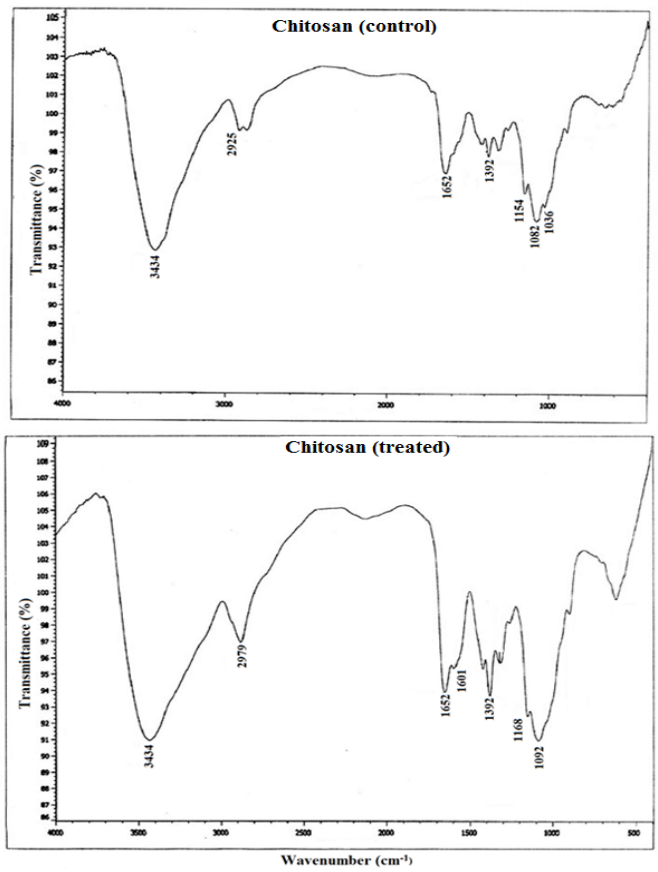

Figure 1: FT-IR spectrum of chitosan (control and treated).

CH stretching, respectively. Another important peak was observed at 1392 cm^{-1}, which indicated the presence of amide-III bending peak. The absorption bands at 1154 cm^{-1} (asymmetric stretching of the –COOC– bridge), 1082, and 1036 cm^{-1} (skeletal vibration involving the COO stretching) were characteristic of its saccharine structure [32].

FT-IR spectrum of treated CS sample showed (Figure 1) $–NH_2$ (amide I) and amide II stretching vibration peaks at 1652 and 1601 cm^{-1}, respectively. Other characteristic peak of -NH stretching vibration peak was observed at 3434 cm^{-1}. The –CH stretching vibration band was shifted from 2925→2979 cm^{-1} and this may be due to increase in bond strength or force constant after biofield treatment. The peaks at 1392, 1168, and 1092 cm^{-1} were due to amide-III bending, asymmetric stretching of the –COOC– bridge and skeletal vibration of -COO stretching.

The IR spectrum of control SA showed (Figure 2) a characteristic peak at 1606 cm^{-1} which was ascribed to carboxylic acid salt (-COO asymmetric stretch, 1500-1650 cm^{-1}). SA showed another important broad peak at 3182 cm^{-1} which was due to inter molecular hydrogen bonded –OH group. The other noticeable peak at 2977 cm^{-1} was due to –CH stretching and -OH bending peaks were observed at 1035, and 1091 cm^{-1} [33]. The biofield treated SA showed (Figure 2) prominent peaks at 1604 cm^{-1}, 3284 cm^{-1} and 2893 cm^{-1} which were mainly due to –COO- group, -OH group and –CH stretching vibration peaks, respectively. Vibration peak for –OH bending was observed at 1037 cm^{-1}. The result showed upward shifting of –OH group from 3182→3284 cm^{-1} which may be due alteration in bond strength. Other FT-IR peaks of treated SA did not show any significant changes with respect to control sample.

CHNSO analysis

CHNSO analysis was used to measure the percentage of elements present in the polymers (CS and SA) and the results are presented in Table 1. The percentage of hydrogen was increased by 16.69% and 46.66% in treated samples of CS and SA, respectively as compared to control. These results indicated that biofield energy was making the hydrogen bond weaker hence facilitating the combustion of hydrogen. Similarly, a significant increase in percentage oxygen was also evidenced in both the polymers, *i.e.*, 11.75%, and 12.05% in CS and SA, respectively. Additionally, the percentage of nitrogen in treated CS was increased (1.82%) as compared to control but no change was observed in SA sample. Likewise, percentage carbon was increased in SA (2.28%) as compared to control though it decreased in case of CS sample

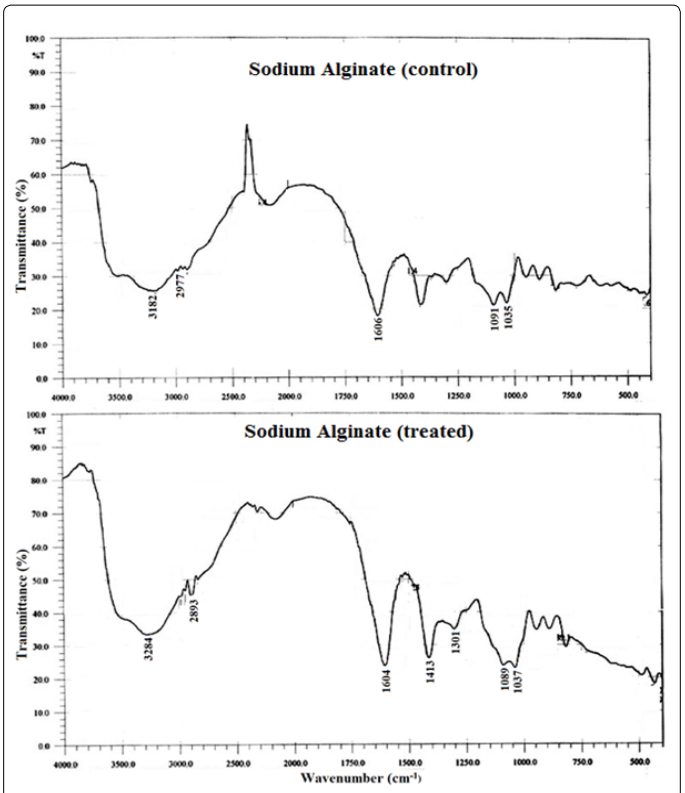

Figure 2: FT-IR spectra of sodium alginate (control and treated).

Elements	Parameter	Chitosan	Sodium Alginate
C	Control	41.93	29.54
	Treated	41.78	30.22
	% Change	-0.35	2.28
H	Control	6.83	3.30
	Treated	7.97	4.84
	% Change	16.69	46.66
N	Control	7.14	0.00
	Treated	7.27	0.00
	% Change	1.82	-
O	Control	30.88	33.65
	Treated	34.51	37.70
	% Change	11.75	12.05

Table 1: CHNSO data of chitosan and sodium alginate.

(-0.35%). It is assumed that biofield treatment may cause substantial increase in percentage of oxygen and hydrogen in both treated natural polymers (CS and SA) with respect to control.

XRD study

Figure 3 shows the XRD diffractogram of control and treated CS. XRD diffractogram of control CS showed more crystalline nature with intense peak at 2θ equals to 19.69°. However, the treated CS showed increase in intensity of the XRD peak and it was observed at 2θ equals to 19.80° (Figure 3). The crystallite size was calculated from the XRD diffractogram of control and treated CS sample using Scherrer formula (crystallite size = kλ /b cos θ) and results are presented in Table 2. The crystallite size of treated CS (18.26 nm) showed significant increase as compared to control CS (10.76 nm). Percentage increase in crystallite size of treated CS was 69.59% as compared to control sample. This may be due to biofield energy which lead to growth in crystal size by removing the inter-crystalline boundaries (grain boundaries) aligning the planes in several adjacent crystals [12].

XRD diffractogram of control and treated SA is shown in Figure 4. XRD of control SA sample showed characteristic semi-crystalline nature with a peak at 2θ equals to 13.61°. Contrarily, the treated SA sample showed more broadening in the XRD peaks. The control SA showed crystallite size of 18.11 nm and treated SA showed crystallite size of 10.68 nm. This showed 41.04% decrease in crystallite size of treated SA as compared to control (Figure 4). Hence, it is assumed that biofield may have significantly changed the crystallite size of treated SA with respect to control. The presence of the internal strain might be the reason for fracturing the grains into sub grains which lead to decrease in crystallite size of treated SA.

Particle size analysis

Particle size (d_{50} and d_{99}) of control and treated SA was investigated

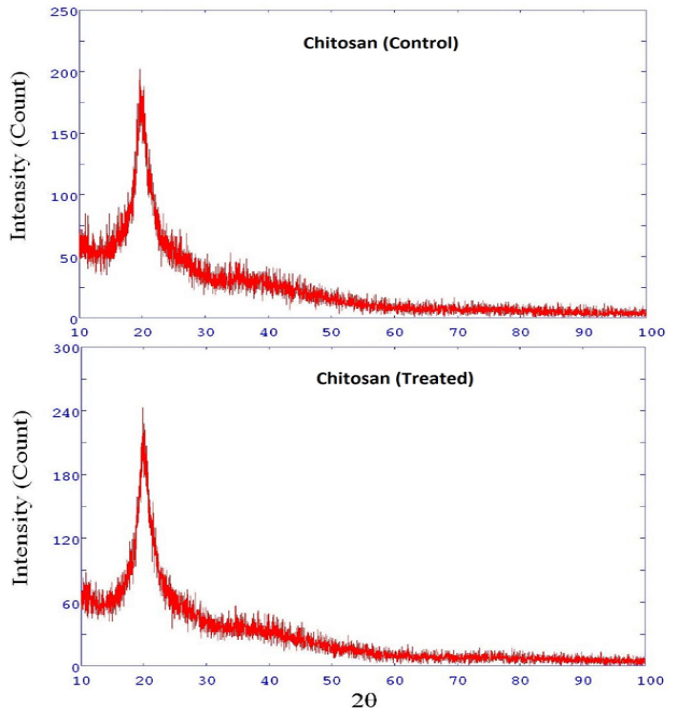

Figure 3: XRD of chitosan (control and treated).

Polymer powder	Crystallite size (nm)		% change in crystallite size
	Control	Treated	
Chitosan	10.76	18.26	69.59
Sodium alginate	18.11	10.68	-41.04

Table 2: Crystallite size and percentage change in crystallite size of polymers (Chitosan and Sodium Alginate).

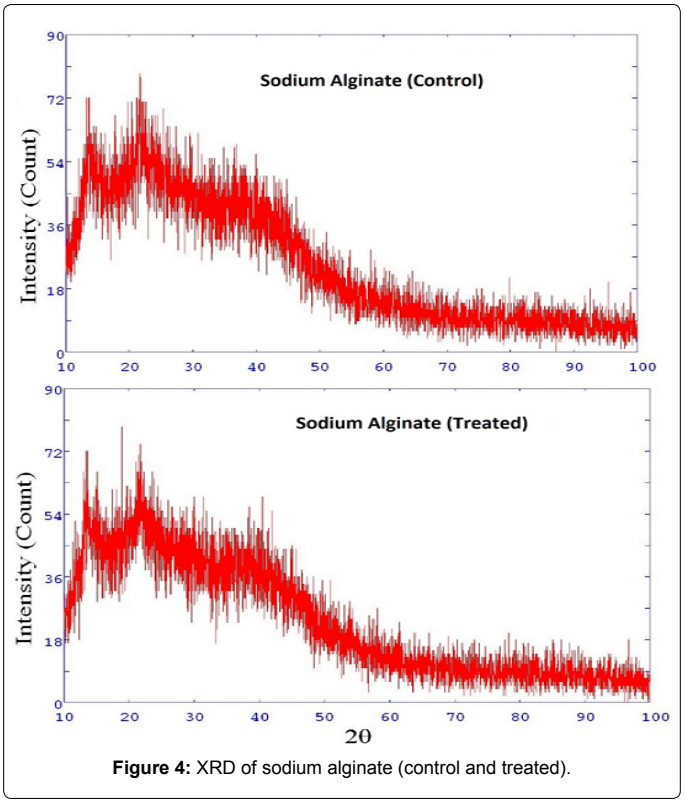

Figure 4: XRD of sodium alginate (control and treated).

and results are presented in Table 3. It was observed that biofield treatment has significantly reduced both average particle size (d_{50}) and d_{99} value of SA polymer with respect to control. The control SA showed a particle size values of d_{50} (65.27 µm) and d_{99} (500 µm). However, after biofield treatment it showed significant reduction in particle size as 11.5 µm and 82.1 µm for d_{50} and d_{99}, respectively. The marked reduction in particle size may be due to the high energy or force experienced by particles which lead to fracture in particle boundaries causing reduction in particle size. Further, it is assumed that too much of plastic deformation due to biofield treatment in samples stores stresses in the form of discontinuities in the particles which ultimately fracture the sample making it much smaller.

Thermal analysis

DSC is an important tool for the determination of glass transition and melting behaviour of polymers. Figure 5 (control, CS T1 and CS T2) shows the DSC thermograms of CS. DSC thermogram of CS sample did not exhibit any glass transition temperature which was mainly associated with its rigid crystalline nature and occurrence of strong inter/intra molecular hydrogen bonding. Kittur et al. suggested that glass transition of CS could lie at a higher temperature where degradation prevents its determination [34]. DSC thermogram of control CS exhibited a broad exothermic peak at 297°C. This exothermic peak can be correlated to decomposition of amine units

Polymer Powder	d_{50} (µm)	d_{99} (µm)
Sodium alginate (control)	65.27	500
Sodium alginate (T1)	11.5	82.1
Chitosan	ND[a]	ND[a]

Table 3: Particle size data (d_{50} and d_{99}) of chitosan and sodium alginate.

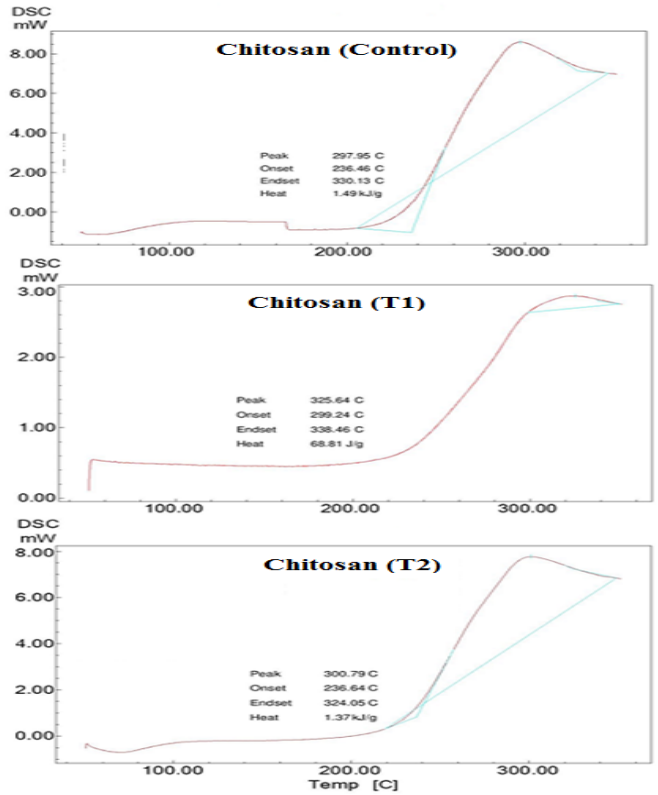

Figure 5: DSC thermogram of control and treated chitosan (T1 and T2).

of the CS sample [34,35]. DSC thermogram of treated CS T1 sample showed (Figure 5) an increase in exothermic temperature peak and it was observed at 325°C. This showed the late decomposition of the amine units of CS T1 with respect to control. DSC thermogram of CS T2 showed an exothermic peak at 300°C. The increase in exothermic decomposition temperature could be associated with strong hydrogen bond formation after biofield treatment in chitosan.

DSC thermogram of SA (Figure 6) (control SA, SA T1 and SA T2) exhibited an endothermic peak at 95°C that may be correlated to elimination of loosely bound water in the control SA. The thermogram showed two exothermic peaks at 241°C and 253°C that was due to pyrolysis reaction in the control SA. Nevertheless, the SA T1 sample also showed an endothermic peak at around 95°C that may be ascribed to bound water in the sample. The DSC thermogram showed (Figure 6) an exothermic peak at 242°C that was ascribed to pyrolysis of the sample. DSC thermogram of SA T2 also showed endothermic peak at around 96°C due to elimination of water. The exothermic event was observed at 243 °C and 269°C and this was due to pyrolysis reaction in the sample [36].

The enthalpy change was calculated from the respective DSC thermograms of control and treated CS and SA polymers (Table 4). The control CS showed an enthalpy value 1490 J/g; however the CS T1 and CS T2 samples showed an enthalpy of 68.81 J/g and 1370 J/g, respectively. However, the control SA showed an enthalpy of 130.93; however the SA T1 and SA T2 samples showed an enthalpy of 499.92 J/g and 272.69 J/g, respectively. The result showed a substantial decrease in enthalpy in treated CS (T1 and T2) by -95.38% and -8.05% with respect to control SA. Whereas, the treated SA showed significant increase in enthalpy by 281.82% and 108.27% with respect to control. Hence, it is assumed that biofield treatment had altered the enthalpy of treated CS and SA as compared to control.

TGA/DTG analysis was conducted on control and treated CS samples and results are presented in Figure 7a and 7b (control, CS T1 and CS T2). CS (control) showed one step thermal degradation pattern. The control CS started to degrade at around 266°C (onset) and degradation terminated at around 350°C. During this thermal process the sample lost 34.70% of its weight. This step was mainly due to CS decomposition and scission of the polymer chain. Derivative thermogravimetry (DTG) graph of control CS exhibited maximum thermal decomposition temperature (T_{max}) at 310°C. However, the treated CS T1 started to decompose at around 236°C and decomposition stopped at around 334°C. The CS T1 lost 43.44% of its weight during

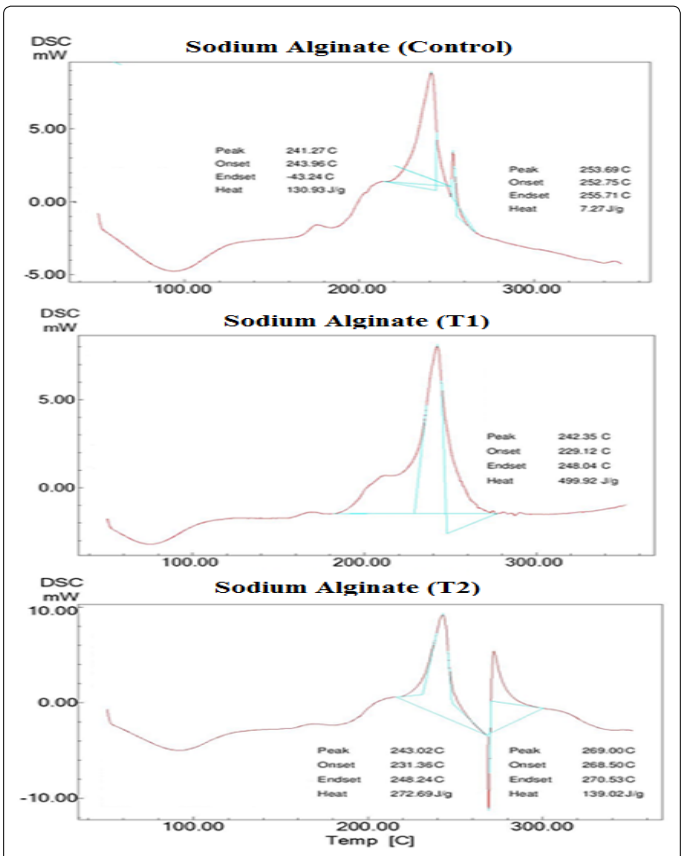

Figure 6: DSC thermogram of control and treated sodium alginate (T1 and T2).

Sample	Chitosan		Sodium Alginate	
	Enthalpy		Enthalpy	
	Value (J/kg)	% change	Value (J/kg)	% change
Control	1490	-	130.93	-
T1	68.81	-95.38	499.92	281.82
T2	1370	-8.05	272.69	108.27

Table 4: Enthalpy change in control and treated chitosan and sodium alginate.

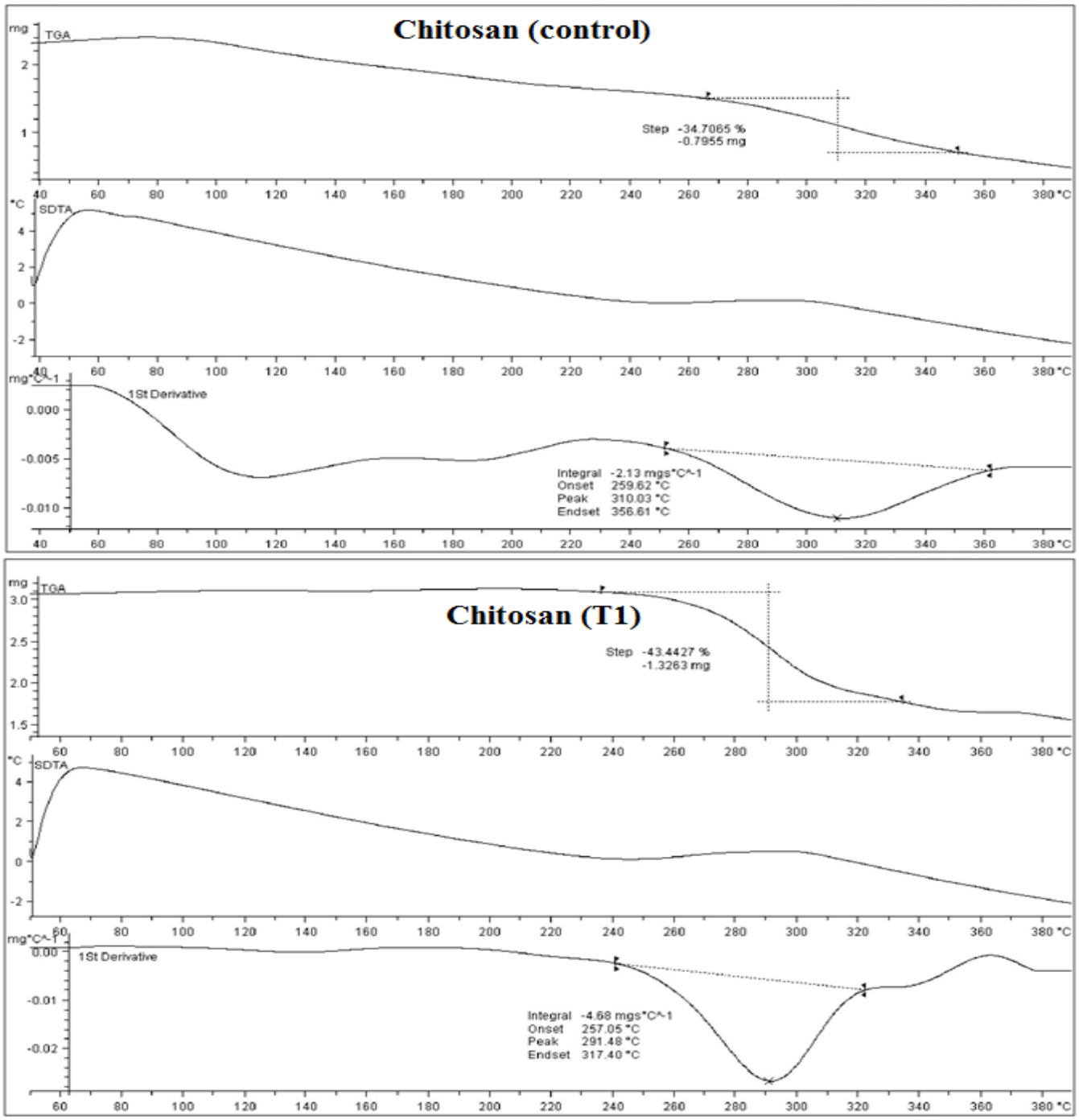

Figure 7a: TGA-DTG thermogram of chitosan (control and T1).

this process. DTG thermogram showed a T_{max} value of 291°C. The TGA thermogram of CS (T2) showed one step thermal degradation (Figure 7b). The degradation commenced at around 259°C and it stopped at around 327°C. During this process CS T2 lost 39.85% of its weight. The DTG showed the T_{max} of 293°C. The comparative evaluation of DTG results showed decrease in T_{max} after biofield treatment of CS. This may be correlated to reduction in thermal stability of CS after biofield treatment.

The TGA-DTG thermogram of control and treated SA (SA T1 and SA T2) are shown in Figure 8a and 8b. The control SA showed one step thermal degradation. The degradation commenced at around 209°C and terminated at around 290°C. During this step the control SA lost 39.11% of its weight. DTG thermogram of control SA showed T_{max} at 240.19°C. The TGA thermogram of SA T1 showed one step thermal degradation. The degradation started at around 192°C and stopped at around 262°C. The SA T1 lost 33.57% of its weight. Based on DTG thermogram of SA T1 the T_{max} was observed at 231°C. The thermal

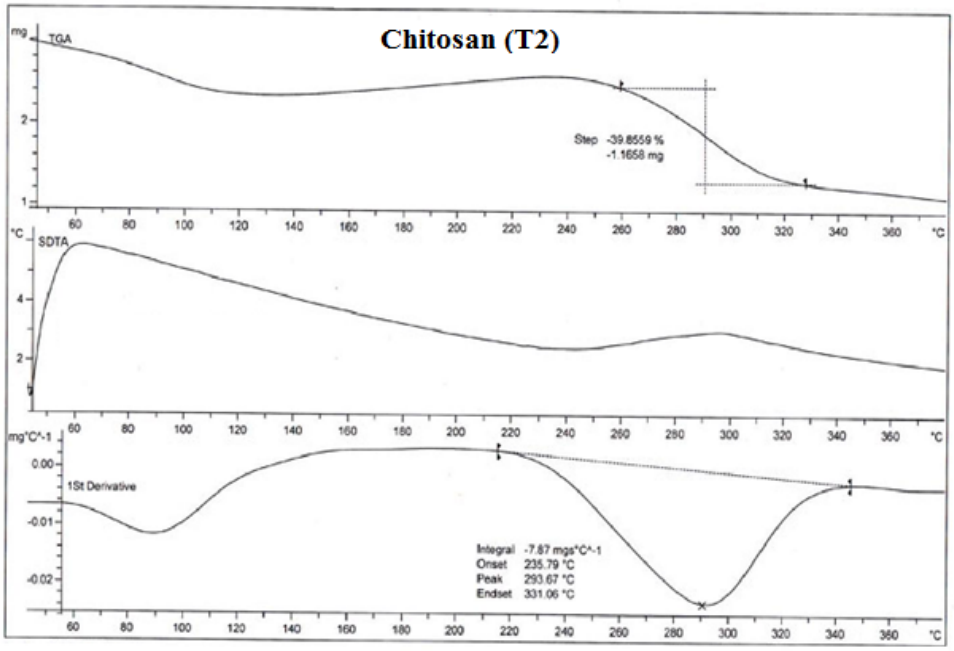

Figure 7b: TGA-DTG thermogram of chitosan (T2).

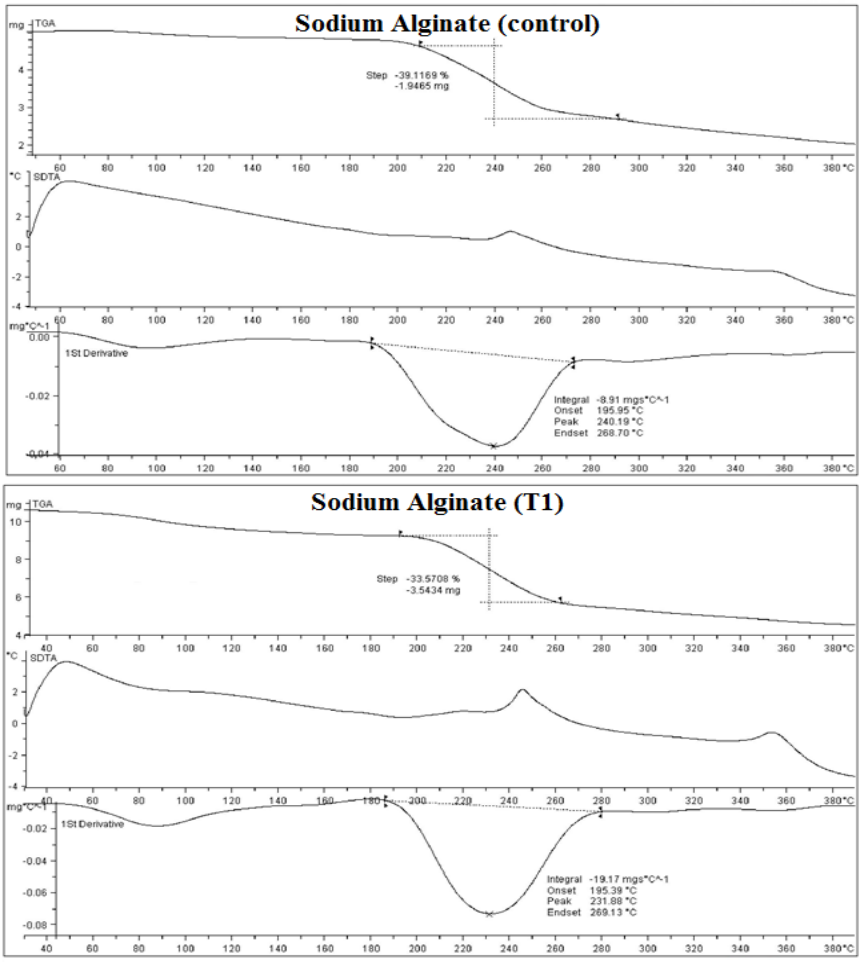

Figure 8a: TGA-DTG thermogram of sodium alginate (control and T1).

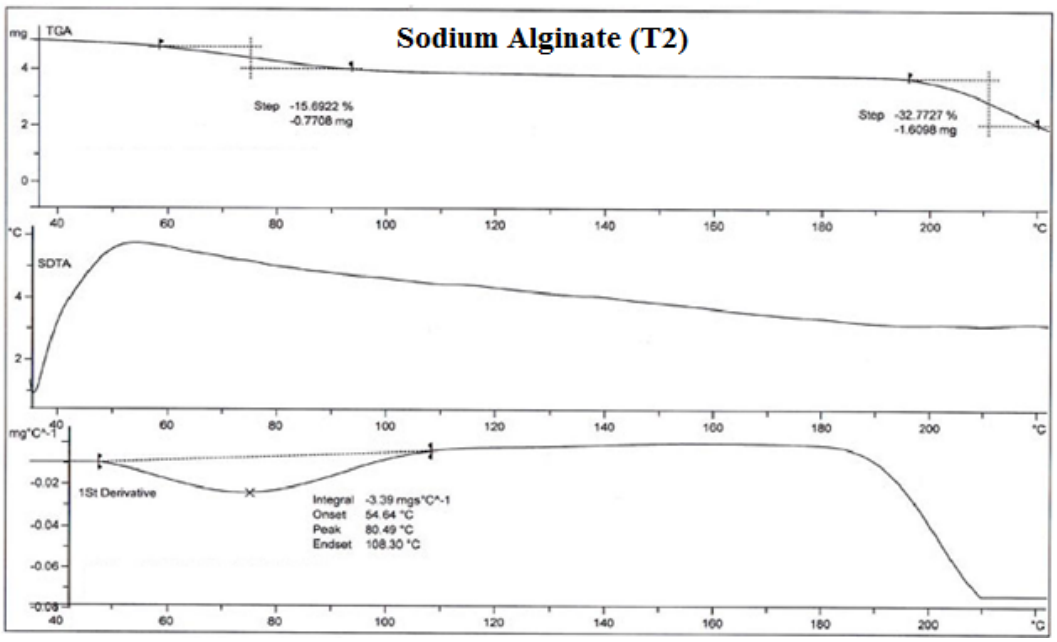

Figure 8b: TGA-DTG thermogram of sodium alginate (T2).

degradation of SA (T2) started at around 196°C and it stopped at around 220°C (Figure 8b). The SA T2 lost 32.77% of its weight during this process. The T_{max} value was decreased in SA T1 as compared to control which correlates with decrease in thermal stability of treated SA with respect to control. This indicated that biofield treatment did not increase the thermal stability of treated SA as compared to control.

Conclusion

This research work showed the impact of biofield treatment on physicochemical and thermal properties of CS and SA. FT-IR study showed increase in wavenumber of –CH stretching vibrations which may be associated with increase in bond strength and force constant. CHNSO analysis showed significant increase in percentage hydrogen and oxygen of treated CS and SA. XRD data revealed the crystalline nature of CS (control and treated) and a significant increase in percentage crystallite size (69.59%) was observed after biofield treatment. However, the treated SA showed decrease in crystallite size by 41.04% as compared to control. The particle size analysis of treated SA showed substantial reduction in particle size with respect to control. DSC study showed increase in exothermic temperature in treated CS which may be related to strong hydrogen bonding in the sample. Similarly increase in exothermic temperature was absorbed in treated SA with respect to control. A significant increase in ΔH was observed in SA T1 by 281.82% and SA T2 by 108.27% with respect to control sample. Moreover, significant change in % enthalpy was evidenced in treated CS with respect to control. TGA results showed reduction in thermal stability of treated polymers (CS and SA) with respect to control. Overall, the results showed that biofield has caused significant impact on physical, chemical and thermal properties of the CS and SA. Hence, it is assumed that biofield treated CS and SA could be used as a matrix for controlled drug delivery systems.

Acknowledgement

We thank Dr. Cheng Dong of NLSC, Institute of Physics, and Chinese academy of Sciences for permitting us to use Powder X software for analysing XRD results. The authors would like to thank Trivedi Science, Trivedi Master Wellness and Trivedi Testimonials for their support during the work.

References

1. Kamel S, Ali N, Jahangir K, Shah SM, El-Gendy AA (2008) Pharmaceutical significance of cellulose: A review. Express Polym Lett 2: 758-778.
2. Alavijeh MS, Chishty M, Qaiser MZ, Palmer AM (2005) Drug metabolism and pharmacokinetics, the blood-brain barrier, and central nervous system drug discovery. NeuroRx 2: 554-571.
3. Ray S, Banerjee S, Maiti S, Laha B, Barik S, et al. (2010) Novel interpenetrating network microspheres of xanthan gum-poly(vinyl alcohol) for the delivery of diclofenac sodium to the intestine--*in vitro* and *in vivo* evaluation. Drug Deliv 17: 508-519.
4. Alderman DA (1984) A Review of cellulose ethers in hydrophilic matrices for oral controlled-release dosage forms. Intern J Pharm Tech Product Manufact 5: 1-9.
5. Heller J (1987) Use of polymers in controlled release of active agents. Controlled Drug Delivery Fundamentals and Applications. Marcel Dekker, New York, 179-212.
6. Longer MA (1990) Sustained-release drug delivery systems. Remington's Pharmaceutical Sciences. Mack Publishing, Easton.
7. Giri TK, Thakur A, Alexander A, Ajazuddin Badwaik H, Tripathi DK (2012) Modified chitosan hydrogels as drug delivery and tissue engineering systems: present status and applications. Acta Pharm Sin B 2: 439-449.
8. Chang CH, Lin YH, Yeh CL, Chen YC, Chiou SF, et al. (2010) Nanoparticles incorporated in pH-sensitive hydrogels as amoxicillin delivery for eradication of *Helicobacter pylori*. Biomacromolecules 11: 133-142.
9. Teli SB, Gokavi GS, Aminabhavi TM (2007) Novel sodium alginate-poly (N-isopropylacrylamide) semi-interpenetrating polymer network membranes for pervaporation separation of water + ethanol mixtures. Sep Purif Technol 56: 150-157.
10. Yang L, Ma X, Guo N (2012) Sodium alginate/Na+-rectorite composite microspheres: preparation, characterization, and dye adsorption. Carbohydr Polym 90: 853-858.
11. Smitha B, Sridhar S, Khan AA (2005) Chitosan–sodium alginate polyion complexes as fuel cell membranes. Eur Polym J 41: 1859-1866.
12. Caykara T, Demirci S, Eroglu MS, Guven O (2005) Poly(ethylene oxide) and its blends with sodium alginate. Polymer 46: 10750-10757.

13. Smidsrod O, Skjak-Braek G (1990) Alginate as immobilization matrix for cells. Trends Biotechnol 8: 71-78.

14. Smidsrod O, Glover RM, Whittington SG (1973) The relative extension of alginate having different chemical composite. Carbohydr Res 27: 107-111.

15. Badwan A, Abumalooh A, Sallam E, Abukalaf A, Jawan O (1985) A sustained release drug delivery system using calcium alginate beads. Drug Dev Ind Pharm 11: 239-256.

16. Aslani P, Kennedy RA (1996) Studies on diffusion in alginate gels. I. Effect of cross-linking with calcium or zinc ions on diffusion of acetaminophen. J Control Release 42: 75-82.

17. Shu XZ, Zhu KJ (2002) The release behavior of brilliant blue from calcium-alginate gel beads coated by chitosan: the preparation method effect. Eur J Pharm Biopharm 53: 193-201.

18. Wang K, He Z (2002) Alginate-konjac glucomannan-chitosan beads as controlled release matrix. Int J Pharm 244: 117-126.

19. LaFleur K, Cassady K, Doud A, Shades K, Rogin E, et al. (2013) Quadcopter control in three-dimensional space using a noninvasive motor imagery-based brain-computer interface. J Neural Eng 10: 046003.

20. Trivedi MK, Patil S, Tallapragada RM (2013) Effect of biofield treatment on the physical and thermal characteristics of vanadium pentoxide powders. J Material Sci Eng S11: 001.

21. Trivedi MK, Patil S, Tallapragada RM (2013) Effect of biofield treatment on the physical and thermal characteristics of silicon, tin and lead powders. J Material Sci Eng 2: 125.

22. Trivedi MK, Patil S, Tallapragada RM (2014) Atomic, crystalline and powder characteristics of treated zirconia and silica powders. J Material Sci Eng 3: 144.

23. Trivedi MK, Patil S, Tallapragada RMR (2015) Effect of biofield treatment on the physical and thermal characteristics of aluminium powders. Ind Eng Manag 4: 151.

24. Shinde V, Sances F, Patil S, Spence A (2012) Impact of biofield treatment on growth and yield of lettuce and tomato. Aust J Basic Appl Sci 6: 100-105.

25. Sances F, Flora E, Patil S, Spence A, Shinde V (2013) Impact of biofield treatment on ginseng and organic blueberry yield. Agrivita J Agric Sci 35: 22-29.

26. Lenssen AW (2013) Biofield and fungicide seed treatment influences on soybean productivity, seed quality and weed community. Agricultural Journal 8: 138-143.

27. Patil SA, Nayak GB, Barve SS, Tembe RP, Khan RR (2012) Impact of biofield treatment on growth and anatomical characteristics of *Pogostemon cablin* (Benth.). Biotechnology 11: 154-162.

28. Nayak G, Altekar N (2015) Effect of biofield treatment on plant growth and adaptation. J Environ Health Sci 1: 1-9.

29. Trivedi MK, Patil S (2008) Impact of an external energy on *Staphylococcus* epidermis [ATCC –13518] in relation to antibiotic susceptibility and biochemical *reactions* – An experimental study. J Accord Integr Med 4: 230-235.

30. Trivedi MK, Patil S (2008) Impact of an external energy on *Yersinia enterocolitica* [ATCC –23715] in relation to antibiotic susceptibility and biochemical reactions: An experimental study. Internet J Alternative Med 6: 2.

31. Trivedi MK, Bhardwaj Y, Patil S, Shettigar H, Bulbule A (2009) Impact of an external energy on *Enterococcus faecalis* [ATCC – 51299] in relation to antibiotic susceptibility and biochemical reactions – An experimental study. J Accord Integr Med 5: 119-130.

32. Peniche C, Arguelles-Monal W, Davidenko N, Sastre R, Gallardo A, et al. (1999) Self-curing membranes of Chitosan/PAA IPNs obtained by Radical Polymerization: Preparation, Characterization and Interpolymer Complexation. Biomaterials 20: 1869-1875.

33. Mishra RK, Ramasamy K, Lim SM, Ismail MF, Majeed AB (2014) Antimicrobial and *in vitro* wound healing properties of novel clay based bionanocomposite films. J Mater Sci Mater Med 25: 1925-1939.

34. Kittur F, Prashanth K, Uday Sankar K, Tharanathan R (2002) Characterization of chitin, chitosan and their carboxymethyl derivatives by differential scanning calorimetry. Carbohydr Polym 49: 185-193.

35. Guinesi LS, Cavalheiro ETG (2006) The use of DSC curves to determine the acetylation degree of chitin/chitosan samples. Thermochim Acta 444: 128-133.

36. Zhou K, Zhang X, Chen Z, Shi L, Li W (2015) Preparation and characterization of hydroxyapatite–sodium alginate scaffolds by extrusion free forming. Ceram Int 41: 14029-14034.

Citation: Jana S, Trivedi MK, Tallapragada RM, Branton A, Trivedi D, Nayak G, et al. (2015) Characterization of Physicochemical and Thermal Properties of Chitosan and Sodium Alginate after Biofield Treatment. Pharm Anal Acta 6: 430. doi:10.4172/21532435.1000430